International Journal of Remote Sensing, 2013
Vol. 34, No. 12, 4449–4465, http://dx.doi.org/10.1080/01431161.2013.779044

Taylor & Francis
Taylor & Francis Group

Impervious surface extraction from high-resolution satellite image using pixel- and object-based hybrid analysis

Xueliang Zhang[a,b], Pengfeng Xiao[a,b]*, and Xuezhi Feng[a,b]

[a]*Department of Geographic Information Science, Nanjing University, Nanjing 210093, PR China;*
[b]*Jiangsu Provincial Key Laboratory of Geographic Information Science and Technology, Nanjing University, Nanjing 210093, PR China*

(*Received 19 December 2011; accepted 18 December 2012*)

High-resolution satellite imaging provides a wealth of details about the Earth's surface, but it is still a challenge to determine the complex, impervious surface from high-resolution satellite images. A pixel- and object-based hybrid analysis (POHA) method is proposed for the extraction task. Pixel-based analysis is first applied to provide prior knowledge; then, based on prior knowledge, the subsequent object-based analysis is simply to find similar rather than new impervious objects using a weighted minimum distance strategy. In order to combine different image analysis methods, the segmentation masking strategy was introduced to transform the image analysis from pixel level to object level. A QuickBird image of Hangzhou City in China was used to test POHA. Furthermore, POHA was compared with both the pixel-based analysis and object-based image analysis (OBIA) methods, showing that POHA runs with limited human–computer interactions, and can provide accurate impervious surface mapping.

1. Introduction

An impervious surface is defined as a material through which water cannot infiltrate into the soil. Impervious surface emerges as a major indicator of urban environment, which mainly focuses on water quality (Schueler 1994; Arnold and Gibbons 1996; Zug et al. 1999; Brabec, Schulte, and Richards 2002; Gillies et al. 2003), rainfall run-off (Brun and Band 2000; Weng 2001; Lohani, Kibler, and Chanat 2002), and urban heat island effect (Weng, Lu, and Schubring 2004; Chen et al. 2006; Yuan and Bauer 2007). Impervious surface also serves as an indicator of urbanization. Timely and accurate information about impervious surface is in great demand for urban planning and management to deal with the numerous problems associated with increasing urbanization (Harbor 1994; Brabec, Schulte, and Richards 2002; Wu and Murray 2005; Lu, Weng, and Li 2006).

Urban areas have substantially different impervious surfaces in terms of types, abundance, and geometry, making it very difficult to extract impervious surface from remote-sensing images. Weng (2012) reviewed various extraction approaches proposed in recent years. According to the suggestion of Jensen and Cowen (1999), spatial resolution is considered more important than spectral resolution in urban mapping. For impervious surface extraction, medium spatial resolution images are widely used, such as Landsat, Satellite Pour l'Observation de la Terre (SPOT), and China–Brazil Earth

*Corresponding author. Email: xiaopf@gmail.com

Resources Satellite (CBERS) images (Wu and Murray 2003; Yang et al. 2003; Lu and Weng 2006, Powell et al. 2007, Pu et al. 2008; Weng and Hu 2008; Luo and Mountrakis 2010; Lu, Hetrick, and Moran 2011a). However, medium resolution is often considered too coarse for fine-scale analysis because of the heterogeneity in urban landscape and the complexity of urban impervious surface materials (Jensen and Cowen 1999; Lu and Weng 2004).

High-spatial resolution images from satellites, such as IKONOS, QuickBird, OrbView, GeoEye, and WorldView, provide a greater potential for extracting more detailed information, and these are increasingly employed for impervious surface mapping. A major advantage of high-resolution satellite images is the reduction in per-pixel spectral heterogeneity. However, the greater level of details would result in higher spectral variance within land-cover units (Hsieh, Lee, and Chen 2001).

Several pixel-based methods have been used to extract impervious surface from high-resolution satellite images, such as the hierarchical fuzzy classification approach using texture and the length–width measure (Shackelford and Davis 2003a), morphological and neural approaches based on image structural information (Benediktsson, Pesaresi, and Arnason 2003), and the decision tree classifier (Lu and Weng 2009). These studies show that the pixel-based analysis method can be used for the extraction task from high-resolution images. But in addition to the spectral features, the shape or structural measures should be involved for better results.

Since the spatial resolution is increased, a ground object would be represented by a set of pixels. The pixel-based analysis method does not make use of spatial concepts and contextual information (Blaschke and Strobl 2001). Moreover, because of the noise involved, the per-pixel-based method could produce a large number of salt-and-pepper pixels (Lu, Moran, and Hetrick 2011b). Because of the limitations of the pixel-based analysis method, the object-based image analysis (OBIA) method is increasingly used for analysing high-resolution images (Benz et al. 2004; Blaschke 2010). The advantages of OBIA are its utilization of spatial and geometrical properties as well as topological features, and the close relation between real-world objects and image objects (Hay and Castilla 2006). Several comparisons have testified that OBIA performs better than the pixel-based method on feature extraction from high-resolution satellite images (Yuan and Bauer 2006; Myint et al. 2011; Pu, Landry, and Yu 2011).

Many successful cases of impervious surface extraction using OBIA have been reported. Zhou and Wang (2008) developed an algorithm of multiple agent segmentation and classification (MASC) including the steps of image segmentation, shadow-effect, MANOVA-based classification, and post-classification. Hu and Weng (2011) proposed an object-based fuzzy classification approach for impervious surface extraction based on spectral, spatial, and textural attributes. In the work of Pu, Landry, and Yu (2011), the artificial neural network (ANN) and minimum distance classifier (MDC) were applied on image objects to obtain detailed urban land cover information. Lu, Moran, and Hetrick (2011b) obtained impervious surface information by classifying the segmentation image into a thematic map using the maximum likelihood classifier (MLC). They also pointed out that the hybrid method involving limited manual editing performed the best.

As described in the cases above, pixel-based supervised classifiers such as ANN, MLC, and MDC can be applied to image objects directly to generate a thematic map. In such cases, a set of object features can be used. For example, in the work of Pu, Landry, and Yu (2011), 27 object features were used when applying ANN and MDC. However, the supervised classification process requires considerable human–computer interaction to select and adjust the training sets. The rule-based or fuzzy rule-based OBIA approach does not need

any training set, and it can make use of the spectral, textual, and contextual attributes of objects in an integrative way. However, the urban landscape is so heterogeneous that the rules are always very complex. Moreover, there are no universal rules qualified to extract the complex impervious surface in various landscape patterns.

Because of the limitations of both the pixel-based analysis and OBIA methods, a pixel- and object-based hybrid analysis (POHA) method is proposed here to extract impervious surface from high-resolution satellite images. Another combined fuzzy pixel- and object-based approach was proposed by Shackelford and Davis (2003b). In their method, the pixel-based classification used was to discriminate roads and buildings from others, and the subsequent object-based analysis was to separate buildings and non-road impervious surface in dense urban areas. Hence, pixel-based classification was not linked to object-based analysis. POHA is different. It is a concise framework aiming at extracting impervious surface. Pixel-based analysis is used to provide prior knowledge for the subsequent object-based analysis. A segmentation masking strategy is proposed to link the two different analysis methods. Hence, the extraction task is divided into two steps. The first, a pixel-based step, is to extract part of the distinct impervious pixels, and the second, an object-based step, is to map all the impervious surfaces using the knowledge gained from the first step. The complexity of both steps is less than simply using only one to perform the extraction task.

Since the key point of this article is not to select robust object features or to define complex rules, only the features of a texture measure and the normalized difference vegetation index (NDVI), and the minimum distance strategy are adopted. In fact, more features, rules, and classifiers can be integrated into POHA to enhance its robustness.

2. Data and study area

A QuickBird image was used to test the proposed POHA method, as shown in Figure 1. It is a subset of the scene in Yuhang District, Hangzhou City, China, which is known as a city from the Liangzhu culture, 3400–2250 BC in the Yangtze River Delta. The scene was acquired on 2 March 2008. The spatial resolution is 2.4 m, and the radiometric resolution is 11 bit. There are four spectral bands: blue, green, red, and near-infrared (NIR). The image size is 937 $\times$ 652 pixels. The test image represents the typical landscape of the newer, small cities in eastern China. Since many new buildings are constructed in farmland, monitoring the impervious surface in such cities is very important for the protection of farmland resources. The test image contains typical land-cover types, such as impervious surface, bare soil, water, shadow, trees, grass, and farmland. It shows great spectral variance from visual analysis (for example, there are many colourful factory rooftops). The tones for roads, parking lots, and recently constructed buildings are different from those of longer-established structures. Spectral variance makes the extraction task very difficult when based only on spectral signatures.

3. Methodology

The flow diagram of POHA is shown in Figure 2. First, a pixel-based analysis was applied to generate the impervious seed pixels, and a parallel image segmentation was implemented to obtain the segmented regions. Then the seed pixels were masked with the segmented regions to produce impervious seed regions. Based on the information of the seed regions, object-based analysis was applied to produce POHA results using the weighted minimum distance strategy. Finally, following POHA, human–computer interaction can be appended to generate the final impervious surface map.

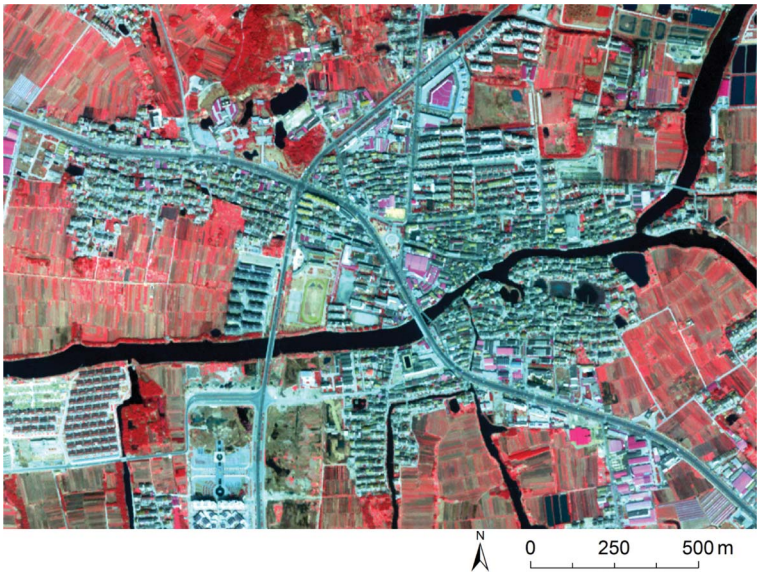

Figure 1. The test QuickBird image in Yuhang District, Hangzhou City, China. The image size is 937 × 652 pixels, shown with a combination of NIR, red, and green bands.

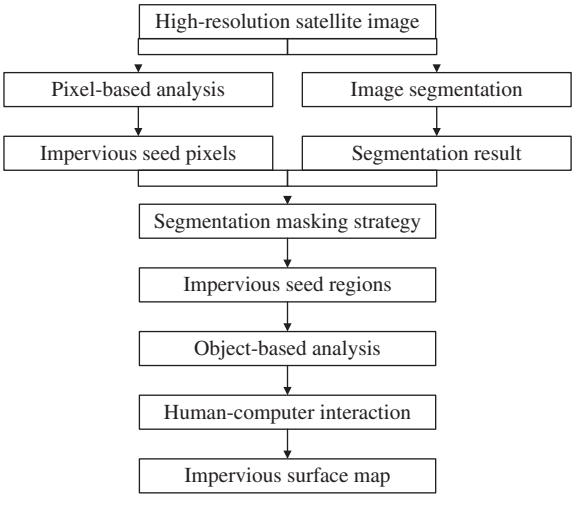

Figure 2. Flow diagram of the pixel- and object-based hybrid analysis (POHA) method.

3.1. Pixel-based analysis for impervious seed pixels

Pixel-based analysis produces impervious seed pixels, serving as the prior knowledge for the subsequent object-based analysis step. It does not aim at extracting all the impervious pixels, simply at identifying accurately part of the distinct impervious pixels as seed pixels.

Since the impervious surface has great spectral variance, a textural attribute (Haralik, Shanmugam, and Dinstein 1973) is used for the extraction task. Textural information is derived from windows of data surrounding the area being analysed, representing the structure information of ground objects. The occurrence texture measure variance (Gonzalez

and Woods 2002) was adopted to indicate the high heterogeneity of the impervious surface. It was calculated from the normalized grey-level histogram $P(z_i)$ of the pixel window $W(z_i)$, where $0 \leq i \leq L-1$, and L is the number of grey levels:

$$\text{Variance} = \sum_{i=0}^{L-1} (z_i - m)^2 p(z_i), \tag{1}$$

where m is the mean value of the grey levels in the window $W(z_i)$:

$$m = \sum_{i=0}^{L-1} z_i p(z_i). \tag{2}$$

According to the definition, variance corresponds to heterogeneity in the window. A sample texture image of variance, which is a subset of the test image, is shown in Figure 3(*b*). The 5×5 pixel window was used to calculate the texture measure. In the texture image, the variance value of impervious surface is larger than others because of the complex structure, but the spatial accuracy of the texture image is not very high. For example, the narrow road in Figure 3(*a*) corresponds to a much wider stripe in Figure 3(*b*). This is because the central pixel is influenced by other pixels in the window when calculating the texture feature.

In order to improve spatial accuracy, the morphological operator of erosion (Gonzalez and Woods 2002) was applied on the texture image. The effect of the erosion operator is twofold: one is that textural values are lowered, and the other is that the effect of high-value texture is reduced. The structuring element was set as 5×5 pixels, which is the same as the window for texture calculation. Figure 3(*c*) shows the eroded result of Figure 3(*b*). The highly textured pixels located near the object boundaries are significantly reduced in the erosion result. For example, the wide stripe in Figure 3(*b*) becomes much narrower in Figure 3(*c*). Then, the object boundaries in the texture image are more congenial to those in the original image. However, besides improving spatial accuracy, the erosion operation could decrease the variance value of some impervious pixels, reducing the discrimination between these and the non-impervious pixels. Then, fewer pixels would be identified as impervious following pixel-based analysis. Since pixel-based analysis just aims at extracting part of the distinct impervious pixels accurately, the erosion operation is preferred for the higher spatial accuracy of the extracted impervious pixels.

The texture image can be calculated based on each spectral band. In order to determine the best band, a textural analysis was performed. For each land-cover type in the test image, a set of sample pixels were selected. The mean variance value of each type was calculated based on the sample pixels, and the result is shown in Figure 4. Figure 4(*a*) is calculated

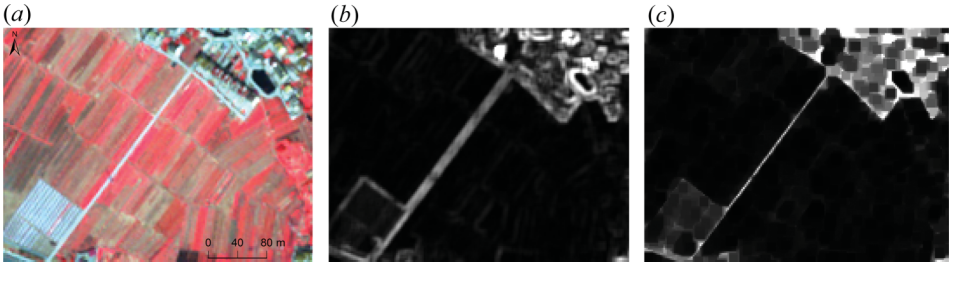

Figure 3. Examples of texture images. (*a*) The original QuickBird image; (*b*) the texture image of variance; and (*c*) the morphologically eroded result of (*b*).

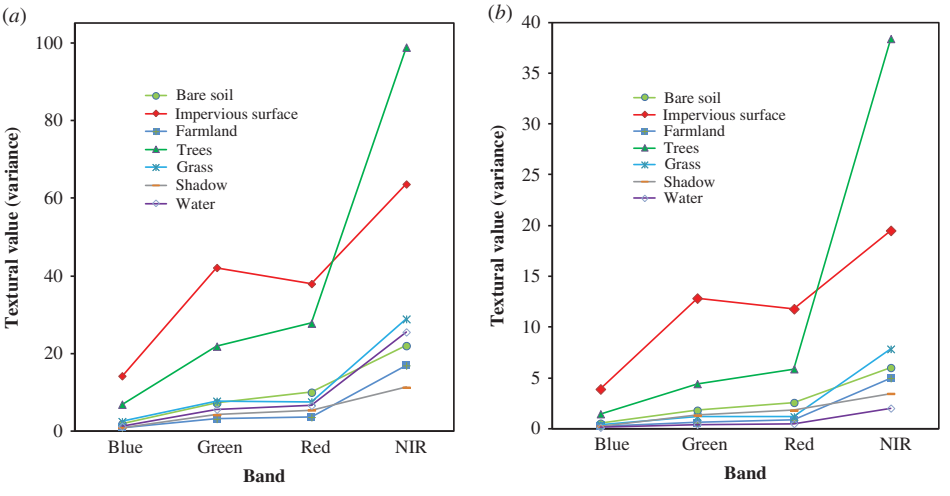

Figure 4. Mean value of the texture measure variance for each land cover type in the test image. (*a*) Calculation based on original texture image and (*b*) calculation based on eroded texture image.

based on the original texture image, and Figure 4(*b*) is calculated based on the eroded texture image. In Figures 4(*a*) and (*b*), the mean variance value of trees in the NIR band is larger than that of impervious surface, but the mean variance value of impervious surface is larger than that of all other land-cover types in the three visible bands. Furthermore, the difference in the green band is the largest among the three visible bands. Thus, in terms of the mean variance value, the green band is better than the other three bands to discriminate impervious surface from others. Comparing Figure 4(*b*) with Figure 4(*a*), the mean variance value of each land-cover type in Figure 4(*b*) is smaller than that in Figure 4(*a*), showing that erosion leads to a decrease in texture value. Nevertheless, the difference between impervious surface and other land-cover types in Figure 4(*b*) is larger than the difference in Figure 4(*a*). Especially for the green band, the mean variance value of impervious surface is about twice as large as that of the trees in Figure 4(*a*), while in Figure 4(*b*), the difference is increased to threefold.

According to the textural analysis above, in order to generate impervious seed pixels, the green band was selected to calculate the variance measure, and the morphological operator of erosion was applied on the texture image. Then, thresholding technology was applied on the eroded texture map to obtain highly textured pixels, which are seen as impervious seed pixels. Unfortunately, there are some tree pixels which still have high texture values. Then, the feature of NDVI was adopted to remove the tree pixels. Pixels with NDVI ≥ 0.1 were excluded from impervious seed pixels.

3.2. Segmentation masking strategy for hybrid analysis

The segmentation masking strategy was used to link the pixel-based analysis and the subsequent object-based analysis. Impervious seed pixels were masked with the segmented regions, and converted to impervious seed regions. Since a region corresponds to an object in the object-based analysis, the analysis is transformed from pixel level to object level.

Image segmentation is to separate an image into a set of spectrally homogeneous and spatially contiguous regions. A bottom-up region-merging method was used to produce

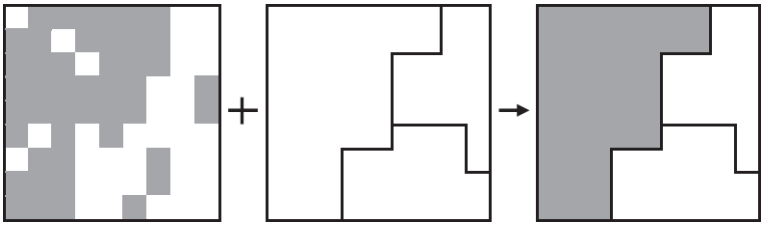

Figure 5. Schematic diagram of the segmentation masking process. (*a*) Map of impervious seed pixels; (*b*) segmentation map with three segmented regions; and (*c*) masking result with one impervious seed region. In (*a*) and (*c*), the grey pixels are identified as impervious pixels.

multi-scale segmentation results, and the local mutual best-merging strategy (Baatz and Schäpe 2000) was then adopted. The merging criterion includes the features of spectral variance, region size, shape property (compactness), and edge strength. It can be viewed as a measure of difference between two adjacent regions. If the measure is small, the corresponding adjacent regions have greater similarity and are more inclined to be merged. The threshold of difference measure is viewed as the scale parameter. Only when the difference measure between two local mutual best-fitted regions is lower than the scale parameter are the two regions allowed to be merged. If the scale parameter is set larger, more merges are allowed to form larger objects, and accordingly, the segmentation scale becomes coarser. Thus, multi-scale segmentations are generated by setting different scale parameters.

The segmentation masking process is shown in Figure 5. The masking strategy is described as that when the map of impervious seed pixels is intersected with the segmentation result, if more than half of the pixels in a segmented region are impervious seed pixels, the region is assigned as an impervious seed region. The advantages of the segmentation masking strategy are concluded as twofold: one is that the salt-and-pepper pixels and tiny holes are removed; the other is the high spatial accuracy of the impervious seed regions. This is because when generating the impervious seed pixels, the boundary of impervious surface is not taken into account. However, the segmentation method can focus on the spatial accuracy of region boundaries. Then, the segmented regions have accurate boundaries, resulting in the high spatial accuracy of impervious seed regions.

3.3. Object-based analysis for impervious surface extraction

The object-based analysis step makes use of the impervious seed regions to identify all the impervious regions. With the benefit of prior knowledge, this involves simply finding the similar rather than the new impervious regions during the object-based analysis process.

In the segmentation result, except for the impervious seed regions, all other regions were assigned as candidate impervious regions (R). The minimum distance strategy was used to determine whether the candidate region belongs to an impervious region. Except for the impervious seed regions and their adjacent regions, all other regions were assigned as non-seed regions. The adjacent regions of seed regions were not included in non-seed regions because they had great potential to be impervious regions. The mean variance value of all seed regions (MV_{seed}) and all non-seed regions ($MV_{nonseed}$) in the green band was calculated. For each candidate region, when its mean variance value (MV_i) in the green band was closer to MV_{seed}, it was assigned as the impervious region; otherwise, it was assigned to the non-impervious regions. In order to make an adjustment, a weight factor (w) was used. Then, the candidate region was assigned as impervious if it satisfied

$$|\mathrm{MV}_i - \mathrm{MV}_{\mathrm{seed}}| < w\,|\mathrm{MV}_i - \mathrm{MV}_{\mathrm{nonseed}}|\,. \tag{3}$$

The weight factor w was introduced because it cannot be taken for granted that the candidate region is impervious or non-impervious when it is nearer to the seed regions or to the non-seed regions. When w is greater than 1, the candidate region could also be assigned as an impervious region even though its distance to impervious seed regions is longer than that to the non-seed regions. On the contrary, when w is less than 1, the candidate region can be assigned as a non-impervious region even though it is nearer to the impervious seed regions.

The object-based analysis process is described as follows.

(1) Find all the candidate impervious regions, impervious seed regions, and non-seed regions. Calculate $\mathrm{MV}_{\mathrm{seed}}$ and $\mathrm{MV}_{\mathrm{nonseed}}$.
(2) If all the candidate regions have been evaluated, terminate the analysis process. Otherwise, find a candidate region (R) which is not evaluated.
(3) If R is nearer to the seed regions, assign it as the impervious region and go to step (4). Otherwise, go back to step (2).
(4) If R belongs to the non-seed regions, remove R from this group to seed regions and update $\mathrm{MV}_{\mathrm{seed}}$ and $\mathrm{MV}_{\mathrm{nonseed}}$. Go back to step (2).

3.4. Human–computer interaction

In POHA, the most impervious regions would be extracted after the object-based analysis step. However, it is difficult to find features sufficiently robust to extract all the complex impervious regions from the high-resolution remote-sensing image. There must be some impervious regions that are not extracted (mis-extracted). In terms of the texture feature variance used in this article, it is insufficiently robust to recognize large homogeneous impervious objects, such as extensive parking lots or factory roofs. In order to further improve the precision of the extracted result, the human–computer interaction is now appended. Manual editing is still needed to generate an impervious surface map with high accuracy (Zhou and Wang 2008; Hu and Weng 2011; Lu, Moran, and Hetrick 2011b). However, we should point out that, even though this step would certainly improve precision, it is not necessary for POHA. In the following Sections 4.2, 4.4, and 5, POHA results are used to describe the output of the object-based analysis step.

Human–computer interaction is also performed at the object level. It is performed iteratively, and each iteration includes two steps. First, select a mis-extracted impervious region. Then, find regions similar to the selected region among the remainder candidate impervious regions, and assign these as impervious regions. Similarity is then evaluated by the spectral distance between two regions. Repeat the select-and-assign process until all impervious regions have been extracted.

4. Results

4.1. Accuracy assessment

Accuracy assessment was conducted based on the reference map, which was produced by manually delineating the impervious surface in the test image, as shown in Figure 6. Comparing the extracted and manually delineated impervious surface pixel by pixel, all pixels in the image were categorized into four types:

Figure 6. Reference map produced by manual delineation. The impervious pixels are marked in white.

(1) *True positive (TP)*: The pixel belongs to impervious surface in both the manual and extracted result.
(2) *True negative (TN)*: The pixel belongs to non-impervious surface in both the manual and extracted result.
(3) *False positive (FP)*: The pixel is incorrectly labelled as impervious in the extracted result.
(4) *False negative (FN)*: The pixel is incorrectly labelled as non-impervious in the extracted result.

Then, based on the number of pixels falling within each category, the measures of producer's accuracy, user's accuracy, overall accuracy, and kappa coefficient were calculated to quantify the extracted results (Foody 2002):

$$\text{Producer's accuracy} = \text{TP}/(\text{TP} + \text{FN}) \text{ or } \text{TN}/(\text{TN} + \text{FP}), \tag{4}$$

$$\text{User's accuracy} = \text{TP}/(\text{TP} + \text{FP}) \text{ or } \text{TN}/(\text{TN} + \text{FN}), \tag{5}$$

$$\text{Overall accuracy} = (\text{TP} + \text{TN})/N, \tag{6}$$

$$\text{Kappa coefficient} = (N(\text{TP} + \text{TN}) - \Sigma)/(N^2 - \Sigma), \tag{7}$$

where $\Sigma = (\text{TP} + \text{FP})\,(\text{TP} + \text{FN}) + (\text{FN} + \text{TN})\,(\text{FP} + \text{TN})$, and N is the total number of pixels.

For producer's accuracy and user's accuracy when the numerator is TP, the measure corresponds to the impervious surface. Otherwise, the measure corresponds to the non-impervious surface.

4.2. Sensitivity of impervious seed pixel to POHA result

In pixel-based analysis, if the textural threshold is set small, more impervious seed pixels are extracted but the number of wrongly extracted (mis-extracted) seed pixels is also

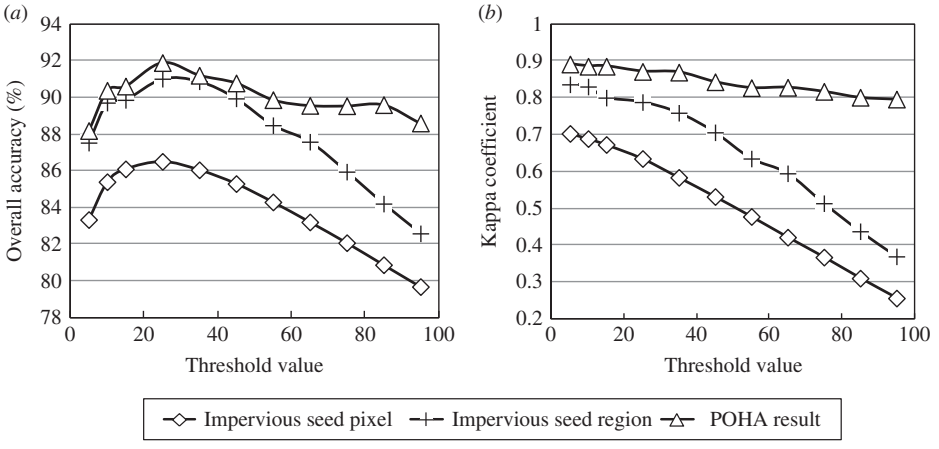

Figure 7. Change in overall accuracy (*a*) and kappa coefficient (*b*) along with the increment in textural threshold value in the pixel-based analysis process.

increased. On the contrary, if the textural threshold is set high, fewer impervious seed pixels are extracted but the number of mis-extracted seed pixels is increased. As shown in Figure 7(*a*), along with the increment in textural threshold, the overall accuracy of the impervious seed pixels initially increased, and then decreased when the textural threshold was higher than 25. However, in Figure 7(*b*), the kappa coefficient steadily decreases with increasing textural threshold.

After segmentation masking, the overall accuracy and kappa coefficient of the impervious seed regions were increased significantly, and the change direction was similar to that of the seed pixels, which shows that better impervious seed pixels would result in seed regions with higher precision. However, it is interesting that in Figure 7(*a*), increments in overall accuracy for impervious seed regions are different. When the textural threshold was 25, the overall accuracy of impervious seed pixels was the highest, and accordingly, the increment was also the greatest, reaching 5%. Then, when the textural threshold was larger or smaller than 25, the overall accuracy of impervious seed pixels decreased gradually, leading to a gradual decline in increment. This indicates that the segmentation masking strategy is sensitive to the accuracy of impervious seed pixels.

In regard to the POHA result after the object-based analysis step, the change direction was similar to that of impervious seed pixels and seed regions, but the range of change was much smaller. Especially when the threshold value is set high, the accuracy of POHA is still high. As shown in Figures 7(*a*) and (*b*), increments in overall accuracy and kappa coefficient increased with increase in threshold value. This is because the object-based analysis step of POHA can help to extract mis-extracted impervious information at an earlier stage. On the other hand, when the threshold value is too small, resulting in too many mis-extracted impervious seed pixels, then the subsequent segmentation masking and object-based analysis step cannot remove the negative influence of such mis-extracted pixels. As shown in Figure 7(*a*), when the threshold is set as 5, since the number of mis-extracted pixels is large, the accuracy of the POHA result is not improved significantly.

According to the analysis above, the POHA result is influenced by the impervious seed pixels, but not very strongly. Impervious seed pixels with higher accuracy would lead to improved POHA. However, when the accuracy of impervious seed pixels is low, the accuracy of POHA result still remains high.

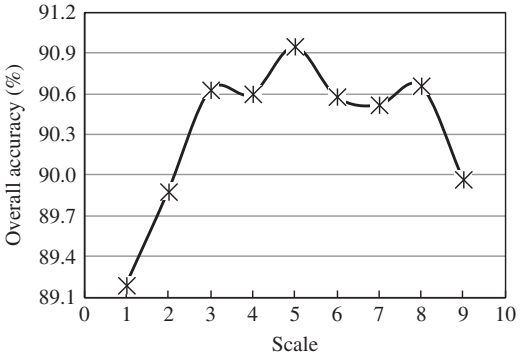

Figure 8. Overall accuracy of the impervious seed regions in multi-scale segmentation masking results. On a scale of 1–9, the segmented regions enlarge as the segmentation scale becomes coarser.

4.3. Effect of segmentation scale on masking result

Since the spatial accuracy of impervious seed regions is dependent on that of segmentation, the segmentation scale would influence the performance of the segmentation masking strategy. Given the impervious seed pixels, a set of multi-scale segmentations were used to produce multi-scale masking results. The performance of the multi-scale masking results was evaluated by the measure of overall accuracy, and the result is shown in Figure 8. On a scale of 1–9, the segmentation will be seen to get coarser. Segmentation at scale 1 is apparently over-segmented with 5334 regions, while that at scale 9 is under-segmented with 329 regions.

As the segmentation scale changes from 1 to 5, the overall accuracy of the masking result is increased but then decreases from 5 to 9. Hence, in terms of the test image, segmentation at scale 5, which has 1069 regions, is best for the masking process in POHA. This is because when segmentation is over-segmented, the relation between image objects and real-world impervious objects is not sufficiently close. Although the number of wrongly segmented pixels is small in the fine-scale segmentation results, the masking process does not perform well. When the segmentation is under-segmented, some wrong merges are allowed to form regions sufficiently large for the large-scale parameter, leading to reduced segmentation precision. Hence, in order to make the masking process perform well, we need to choose a suitable segmentation scale that is neither too coarse nor too fine.

4.4. Comparing POHA with OBIA and pixel-based analysis

The intermediate and final results of POHA are shown in Figure 9. In Figure 9(*a*), the pixel-based analysis result was produced by setting the texture threshold at 25 according to the analysis in 4.2, serving as the impervious seed pixels. From visual assessment, there were many meaningless salt-and-pepper impervious pixels and tiny holes in the result, and some impervious regions were fragmentized because of spectral variance. In Figure 9(*b*), segmentation with 1069 regions is shown, which performed best according to the analysis in 4.3. The segmentation masking result is shown in Figure 9(*c*). Once the impervious seed pixels were transformed to seed regions, the meaningless impervious pixels and tiny holes were removed and the outlines of impervious surface became more regular than those in Figure 9(*a*). Based on prior knowledge from Figure 9(*c*), object-based analysis was performed to produce the POHA result, as shown in Figure 9(*d*). The distance weight was

Figure 9. Impervious surface extraction results of the test image. (*a*) Pixel-based analysis result representing impervious seed pixels; (*b*) segmentation result with 1069 regions; (*c*) segmentation masking result representing impervious seed regions; (*d*) POHA result after object-based analysis; (*e*) final impervious map following human–computer interaction; and (*f*) OBIA result for comparison. In (*a*), (*c*), (*d*), (*e*), and (*f*), the white pixels are identified as impervious.

set at 2.5 after the trial-and-error process. The final impervious map following human–computer interaction is shown in Figure 9(*e*). From Figure 9(*c*) to (*d*), and to Figure 9(*e*), the mis-extracted impervious regions are gradually complemented.

The result obtained using only the OBIA method is shown in Figure 9(*f*) for comparison. The same segmentation result as that for POHA is used for OBIA, and the rules are the same as those for pixel-based analysis. For each region, when the mean texture measure in the green band is larger than 25 and the mean NDVI value is less than 0.1, it is assigned as the impervious region.

Table 1. Accuracy assessment results of Figure 9.

Results of different methods	Producer's accuracy (%)	User's accuracy (%)	Overall accuracy (%)	Kappa coefficient
Pixel-based analysis result				
Impervious	81.9	90.1	86.5	0.63
Non-impervious	91.0	83.5		
Segmentation masking result				
Impervious	89.5	92.1	90.9	0.79
Non-impervious	92.4	89.7		
POHA result				
Impervious	93.8	90.3	91.9	0.87
Non-impervious	90.0	93.6		
OBIA result				
Impervious	88.8	89.0	89.0	0.77
Non-impervious	89.1	88.9		

The accuracy assessment results of the POHA and OBIA results in Figure 9 are shown in Table 1. After the transformation of impervious seed pixels to seed regions, all four accuracy measures were significantly improved. Especially, the producer's accuracy of impervious surface increased by 7.6% and the overall accuracy and kappa coefficient were improved by 4.5% and 0.16, respectively. In terms of the POHA result, these improvements are not as significant as those of the previous step. Although the producer's accuracy of the impervious surface was increased by 4.31%, the overall accuracy and kappa coefficient were increased by 0.9% and 0.08, respectively. This is because the best textural threshold and the best segmentation scale helped to extract most of the impervious surfaces, and there were not many mis-extracted impervious regions before the object-based analysis. Since only a few impervious regions were mis-extracted after the object-based analysis step, the effectiveness of human–computer interaction is even less significant than the object-based analysis step. The overall accuracy increased by 0.8% and the kappa coefficient was only 0.03 higher, reaching 92.7% and 0.9, respectively.

In regard to comparison of POHA with OBIA and pixel-based analysis, the results in Figures 9(*d*), (*f*), and (*a*) were used, respectively. From visual analysis, the pixel-based analysis result is more fragmented than the POHA and OBIA results. Comparing the POHA result with the OBIA result, more impervious objects were mis-extracted in the OBIA result, and some water areas were incorrectly labelled as impervious surface in OBIA. Moreover, the accuracy assessment results in Table 1 also show that POHA performed better than either of the other methods, and OBIA was better than pixel-based analysis.

5. Discussion and conclusions

A POHA method is proposed to extract impervious surface from high-resolution satellite images. POHA integrates the pixel- and object-based analysis method into a concise framework. First, pixel-based analysis was applied to produce impervious seed pixels based on the morphologically eroded texture image. Second, a segmentation masking strategy was introduced to transform the seed pixels into impervious seed regions, which serve as the prior knowledge in the next step. Finally, object-based analysis was applied to find other impervious regions similar to the prior knowledge using the weighted minimum distance strategy. Following POHA, limited human–computer interaction was appended to produce

the final impervious surface map. Taking the QuickBird image of Hangzhou City in China as the test image, the overall accuracy of the POHA result is 91.9%, with a kappa coefficient of 0.87. It was also shown that POHA performs better than OBIA and pixel-based analysis in the experiment.

The occurrence texture measure variance was adopted in this article. Textural analysis shows that the green band performed best among all four bands in terms of the QuickBird test image. Moreover, the morphological operator of erosion was applied on the texture map, which helped to improve spatial accuracy and the ability to discriminate impervious surface from others.

Usually, the extraction task is achieved by using either OBIA or the pixel-based analysis method independently. In POHA, however, this task is jointly fulfilled by the pixel-based analysis step and the OBIA step, and complexity is reduced compared with using only one of the two methods. In POHA, pixel-based analysis does not aim at extracting all impervious pixels, but simply producing impervious seed pixels as accurately as possible. According to the experiment in Section 4.2, the sensitivity of impervious seed pixels to the POHA result is not very strong. But the mix-extracted, rather than mis-extracted impervious seed pixels should be avoided because only the mis-extracted impervious pixels can be remedied in subsequent steps. Hence, in the pixel-based analysis process, a larger textural threshold is preferred.

With the benefit of prior knowledge from previous steps, object-based analysis is directed toward finding other similar impervious regions. Furthermore, the segmentation masking strategy also helps to improve the accuracy of the extracted result. In Figure 9, the pixel-based analysis and OBIA results are set at the same texture threshold, but both the overall accuracy and kappa coefficient of the segmentation masking result are higher than those of the OBIA result. Especially, the overall accuracy of the masking result is 2% higher than that of the OBIA result. The performance of the masking strategy depends on the quality and scale of the segmentation result. According to the analysis in the experiment, we suggest that segmentation should be neither over-segmented nor under-segmented.

In the segmentation masking strategy, if more than half of the pixels in a segmented region are impervious, then the region is assigned as an impervious region. Other thresholds can be set to determine the impervious seed region for various study areas. No matter how one determines the threshold, there would be concerns that some impervious objects might be removed by the segmentation masking strategy because in such regions the number of impervious pixels is less than the threshold. In this case, subsequent object-based analysis would help to extract these impervious objects that had been omitted. Another concern in regard to the segmentation masking strategy is that the impervious seed regions identified do not have 100% impervious pixels because the seed regions are determined by part of the pixels in the region. This concern can be eliminated by ensuring that the segmented regions correspond closely to the real-world impervious object.

Since the key point of the article is to introduce the framework of POHA, the rules and features adopted are quite simple. Only the features of the textural measure variance and NDVI, and the thresholding strategy are used in the pixel-based analysis process. In the subsequent object-based analysis process, only the texture measure and weighted minimum distance strategy are used. In particular, the same texture feature is used in both the pixel- and the object-based analysis steps. If different effective features are used in the two steps, POHA would perform better. Although the extracted POHA result is favourable, further features and rules could be integrated in POHA, such as spectral signature, shape, contextual information, and the rules of region growing, unsupervised classifier, and fuzzy rules. After expansion, POHA could handle images with higher spatial resolution and various landscapes. Moreover, POHA is not restricted to the task of impervious surface extraction:

it can be qualified to extract other ground objects on high-resolution images. Hence, in the future, we will try to further improve the robustness of POHA.

Acknowledgements

This work was supported by the National Basic Research Programme of China (Grant No. 2011CB952001), the Special Fund for Scientific Research of Non-Profit Industry of Ministry of Land and Resources of China (Grant No. 201011015–1), and a project funded by the Priority Academic Programme Development of Jiangsu Higher Education Institutions. The authors would like to thank the anonymous referees for their contributory comments.

References

Arnold, C. L., and C. J. Gibbons. 1996. "Imperious Surface Coverage: The Emergence of a Key Environmental Indicator." *Journal of the American Planning Association* 62: 243–258.

Baatz, M., and M. Schäpe. 2000. "Multiresolution Segmentation – An Optimization Approach for High Quality Multi-Scale Image Segmentation." In *Angewandte Geographische Informations-Verarbeitung XII*, edited by J. Strobl, T. Blaschke, and G. Griesebner, 12–23. Karlsruhe: Wichmann Verlag.

Benediktsson, J. A., M. Pesaresi, and K. Arnason. 2003. "Classification and Feature Extraction for Remote Sensing Images from Urban Areas Based on Morphological Transformations." *IEEE Transactions on Geoscience and Remote Sensing* 41: 1940–1949.

Benz, U. C., P. Hofmann, G. Willhauck, I. Lingenfelder, and M. Heynen. 2004. "Multi-Resolution, Object-Oriented Fuzzy Analysis of Remote Sensing Data for GIS-Ready Information." *ISPRS Journal of Photogrammetry & Remote Sensing* 58: 239–258.

Blaschke, T. 2010. "Object Based Image Analysis for Remote Sensing." *ISPRS Journal of Photogrammetry and Remote Sensing* 65: 2–16.

Blaschke, T., and J. Strobl. 2001. "What's Wrong with Pixels? Some Recent Developments Interfacing Remote Sensing and GIS." *GIS-Zeitschrift Für Geoinformationssysteme* 14: 12–17.

Brabec, E., S. Schulte, and P. L. Richards. 2002. "Impervious Surface and Water Quality: A Review of Current Literature and Its Implications for Watershed Planning." *Journal of Planning Literature* 16: 499–514.

Brun, S. E., and L. E. Band. 2000. "Simulating Runoff Behavior in an Urbanizing Watershed." *Computers, Environment and Urban Systems* 24: 5–22.

Chen, X., H. Zhao, P. Li, and Z. Yin. 2006. "Remote Sensing Image-Based Analysis of the Relationship between Urban Heat Island and Land Use/Cover Changes." *Remote Sensing of Environment* 104: 133–146.

Foody, G. M. 2002. "Status of Land Cover Classification Accuracy Assessment." *Remote Sensing of Environment* 80: 185–201.

Gillies, R. R., J. B. Box, J. Symanzik, and E. J. Rodemaker. 2003. "Effects of Urbanization on the Aquatic Fauna of the Line Creek Watershed, Atlanta – A Satellite Perspective." *Remote Sensing of Environment* 86: 411–422.

Gonzalez, R. C., and R. E. Woods. 2002. *Digital Image Processing*. 2nd ed. Upper Saddle River, NJ: Prentice-Hall.

Haralik, R. M., K. Shanmugam, and I. Dinstein. 1973. "Textural Features for Image Classification." *IEEE Transitions on Systems, Man and Cybernetics* SMC-3: 610–621.

Harbor, J. M. 1994. "A Practical Method for Estimating the Impact of Land Use Change on Surface Runoff, Groundwater Recharge and Wetland Hydrology." *American Planning Association* 60: 95–108.

Hay, G. J., and G. Castilla. 2006. "Object-Based Image Analysis: Strengths, Weaknesses, Opportunities and Threats (SWOT)." Accessed February 23, 2012. http://www.isprs.org/proceedings/XXXVI/4-C42/Papers/01_Opening%20Session/OBIA2006_Hay_Castilla.pdf

Hsieh, P. F., L. C. Lee, and N. Chen. 2001. "Effect of Spatial Resolution on Classification Errors of Pure and Mixed Pixels in Remote Sensing." *IEEE Transactions on Geoscience and Remote Sensing* 39: 2657–2663.

Hu, X., and Q. Weng. 2011. "Impervious Surface Area Extraction from IKONOS Imagery Using an Object-Based Fuzzy Method." *Geocarto International* 26: 3–20.

Jensen, J. R., and D. C. Cowen. 1999. “Remote Sensing of Urban/Suburban Infrastructure and Socioeconomic Attributes.” *Photogrammetric Engineering and Remote Sensing* 65: 611–622.

Lohani, V., D. F. Kibler, and J. Chanat. 2002. “Constructing a Problem Solving Environment Tool for Hydrologic Assessment of Land Use Change.” *Journal of the American Water Resources Association* 38: 439–452.

Lu, D., S. Hetrick, and E. Moran. 2011a. “Detection of Impervious Surface Change with Multitemporal Landsat Images in an Urban–Rural Frontier.” *ISPRS Journal of Photogrammetry and Remote Sensing* 66: 298–306.

Lu, D., E. Moran, and S. Hetrick. 2011b. “Impervious Surface Mapping with Quickbird Imagery.” *International Journal of Remote Sensing* 32: 2519–2533.

Lu, D., and Q. Weng. 2004. “Spectral Mixture Analysis of the Urban Landscapes in Indianapolis with Landsat ETM+ Imagery.” *Photogrammetric Engineering and Remote Sensing* 70: 1053–1062.

Lu, D., and Q. Weng. 2006. “Use of Impervious Surface in Urban Land Use Classification.” *Remote Sensing of Environment* 102: 146–160.

Lu, D., and Q. Weng. 2009. “Extraction of Urban Impervious Surfaces from an IKONOS Image.” *International Journal of Remote Sensing* 30: 1297–1311.

Lu, D., Q. Weng, and G. Li. 2006. “Residential Population Estimation Using a Remote Sensing Derived Impervious Surface Approach.” *International Journal of Remote Sensing* 27: 3553–3570.

Luo, L., and G. Mountrakis. 2010. “Integrating Intermediate Inputs from Partially Classified Images within a Hybrid Classification Framework: An Impervious Surface Estimation Example.” *Remote Sensing of Environment* 114: 1220–1229.

Myint, S. W., P. Gober, A. Brazel, S. Grossman-Clarke, and Q. Weng. 2011. “Per-Pixel vs. Object-Based Classification of Urban Land Cover Extraction Using High Spatial Resolution Imagery.” *Remote Sensing of Environment* 115: 1145–1161.

Powell, R. L., D. A. Roberts, P. E. Dennison, and L. L. Hess. 2007. “Sub-Pixel Mapping of Urban Land Cover Using Multiple End-Member Spectral Mixture Analysis: Manaus, Brazil.” *Remote Sensing of Environment* 106: 253–267.

Pu, R., P. Gong, R. Michishita, and T. Sasagawa. 2008. “Spectral Mixture Analysis for Mapping Abundance of Urban Surface Components from the Terra/ASTER Data.” *Remote Sensing of Environment* 112: 939–954.

Pu, R., S. Landry, and Q. Yu. 2011. “Object-Based Urban Detailed Land Cover Classification with High Spatial Resolution IKONOS Imagery.” *International Journal of Remote Sensing* 32: 3285–3308.

Schueler, T. R. 1994. “The Importance of Imperviousness.” *Watershed Protection Techniques* 1: 100–111.

Shackelford, A. K., and C. H. Davis. 2003a. “A Hierarchical Fuzzy Classification Approach for High-Resolution Multispectral Data Over Urban Areas.” *IEEE Transactions on Geoscience and Remote Sensing* 41: 1920–1932.

Shackelford, A. K., and C. H. Davis. 2003b. “A Combined Fuzzy Pixel-Based and Object-Based Approach for Classification of High-Resolution Multispectral Data over Urban Areas.” *IEEE Transactions on Geoscience and Remote Sensing* 41: 2354–2364.

Weng, Q. 2001. “Modeling Urban Growth Effect on Surface Runoff with the Integration of Remote Sensing and GIS.” *Environmental Management* 28: 737–748.

Weng, Q. 2012. “Remote Sensing of Impervious Surfaces in the Urban Areas: Requirements, Methods, and Trends.” *Remote Sensing of Environment* 117: 34–49.

Weng, Q., and X. Hu. 2008. “Medium Spatial Resolution Satellite Imagery for Estimating and Mapping Urban Impervious Surfaces Using LSMA and ANN.” *IEEE Transactions on Geoscience and Remote Sensing* 46: 2397–2406.

Weng, Q., D. Lu, and J. Schubring. 2004. “Estimation of Land Surface Temperature-Vegetation Abundance Relationship for Urban Heat Island Studies.” *Remote Sensing of Environment* 89: 467–483.

Wu, C., and A. T. Murray. 2003. “Estimating Impervious Surface Distribution by Spectral Mixture Analysis.” *Remote Sensing of Environment* 84: 493–505.

Wu, C., and A. T. Murray. 2005. “A Cokriging Method for Estimating Population Density in Urban Areas.” *Computers, Environment and Urban Systems* 29: 558–579.

Yang, L., C. Huang, C. Homer, B. Wylie, and M. Coan. 2003. "An Approach for Mapping Large-Area Impervious Surface: Synergistic Use of Landsat 7 ETM+ and High Spatial Resolution Imagery." *Canadian Journal of Remote Sensing* 29: 230–240.

Yuan, F., and M. E. Bauer. 2006. "Mapping Impervious Surface Area Using High Resolution Imagery: A Comparison of Object-Based and per Pixel Classification." American Society for Photogrammetry and Remote Sensing Annual Conference Proceedings, Reno, Nevada, USA, May 1–5.

Yuan, F., and M. E. Bauer. 2007. "Comparison of Impervious Surface Area and Normalized Difference Vegetation Index as Indicators of Surface Urban Heat Island Effects in Landsat Imagery." *Remote Sensing of Environment* 106: 375–386.

Zhou, Y., and Y. Q. Wang. 2008. "Extraction of Impervious Surface Areas from High Spatial Resolution Imagery by Multiple Agent Segmentation and Classification." *Photogrammetric Engineering & Remote Sensing* 74: 857–868.

Zug, M., L. Phan, D. Bellefleur, and O. Scrivener. 1999. "Pollution Wash-Off Modeling on Impervious Surface: Calibration, Validation and Transposition." *Water Science and Technology* 39: 17–24.